Full Length Article

Development of empirical relationships for prediction of mechanical and wear properties of AA6082 aluminum matrix composites produced using friction stir processing

CrossMark

I. Dinaharan [a,*], N. Murugan [b], A. Thangarasu [c]

[a] Department of Mechanical Engineering Science, University of Johannesburg, Auckland Park Kingsway Campus, Johannesburg 2006, South Africa
[b] Department of Mechanical Engineering, Coimbatore Institute of Technology, Coimbatore, Tamil Nadu 641014, India
[c] Department of Mechanical Engineering, Sri Ramakrishna Institute of Technology, Coimbatore, Tamil Nadu 641010, India

ABSTRACT

Friction Stir Processing (FSP) has been established as a potential solid state production method to prepare aluminum matrix composites (AMCs). FSP was effectively applied to produce AA6082 AMCs reinforced with various ceramic particles such as SiC, Al_2O_3, TiC, B_4C and WC in this work. Empirical relationships were estimated to predict the influence of FSP process parameters on the properties such as area of stir zone, microhardness and wear rate of AMCs. FSP experiments were executed using a central composite rotatable design consisting of four factors and five levels. The FSP parameters analyzed were tool rotational speed, traverse speed, groove width and type of ceramic particle. The effect of those parameters on the properties of AMCs was deduced using the developed empirical relationships. The predicted trends were explained with the aid of observed macro and microstructures.

© 2016 Karabuk University. Publishing services by Elsevier B.V. This is an open access article under the CC BY-NC-ND license (http://creativecommons.org/licenses/by-nc-nd/4.0/).

1. Introduction

Aluminum matrix composites AMCs have evolved as potential materials to alternate conventional monolithic aluminum alloys in many applications owing to its high specific strength and stiffness, low density, low thermal expansion coefficient and high wear resistance. AMCs are used in numerous industries that are not limited to aerospace, automotive, defense, naval, electronic packaging, thermal and sports [1–4]. Nevertheless, the production of AMCs remains a challenging task to achieve high performance and service life. Liquid metallurgy routes are commonly adopted to produce AMCs due to its simplicity and applicability to mass production [5,6]. But several defects such as poor wettability, interfacial reactions, decomposition of ceramic particles, porosity and poor distribution are encountered [7–9].

Friction stir processing (FSP) is a novel solid state method to produce AMCs and a promising method to overcome the limitations of liquid metallurgy routes [10–12]. The ceramic particles are packed along the tool travel direction using various methods including vertical cylindrical holes [13], square grooves [14] and V shaped grooves [15]. The frictional heat developed by the rotating

shoulder and the pin plasticizes the aluminum alloy. The transverse movement of the tool causes the transportation of plasticized material from advancing side to retreading side. Subsequently the groove portion crumbles and the stirring action of the tool disperses the packed ceramic particles into the plasticized aluminum alloy. The AMCs is thus formed and forged at the back of the tool due to the applied axial force [16,17].

Some studies on production of AMCs using FSP were reported in literatures [18–24]. Mahmoud et al. [18] investigated the role of tool rotational speed, traverse speed and number of passes on the distribution of AA1050/SiC AMCs. Lim et al. [19] found that increasing the tool rotation speed improved the homogeneity of nanotubes in AA6111/CNT AMCs. Kurt et al. [20] reported that tool rotational speed and traverse speed significantly affect the thickness of composite layer, grain size and distribution of reinforcements in AA1050/SiC AMCs. Salehi et al. [21] optimized the FSP process parameters to produce AA6061/SiC using Taguchi parametric design approach. Moghaddas and Bozorg [22] stated that rotational speed is more effective on stirred zone area than traverse speed in AA5754/Si_3N_4 AMCs. Devaraju et al. [23] attempted to optimize the FSP parameters to produce high wear resistant AA6061/(SiC + Gr) hybrid AMCs. Bahrami et al. [24] showed that the traverse speed controls the grain size and tensile strength of AA7075/SiC nano AMCs.

The majority of the published literature focused on the effect of one or few FSP parameters on microstructure, hardness, tensile strength and wear rate. SiC and Al_2O_3 particles at nano and micro levels were
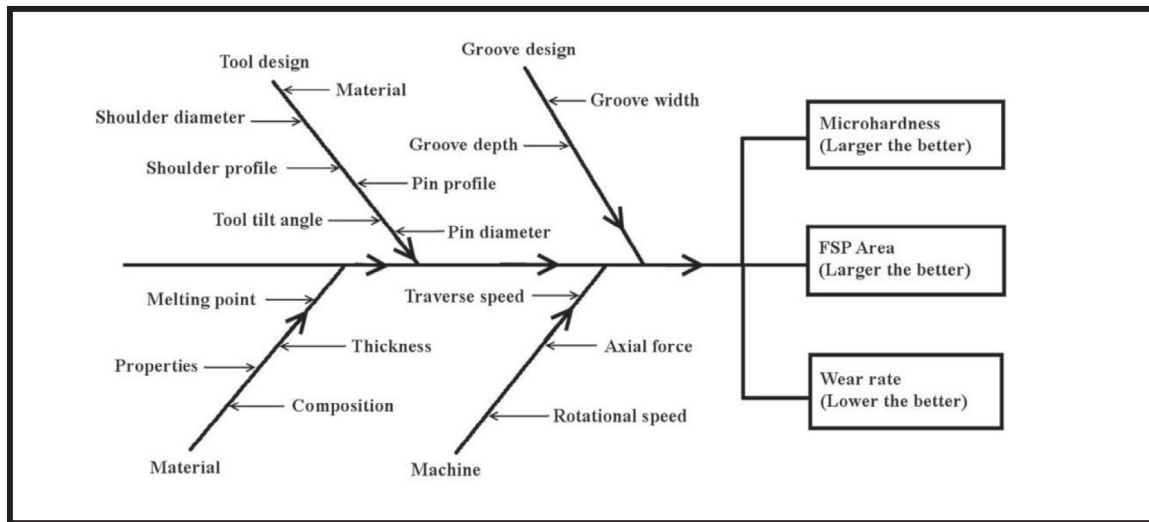
Fig. 1. FSP parameters influencing the properties of surface composite.

used predominantly for producing AMCs using FSP. Therefore, an attempt has been made to develop empirical relationships to predict the stir zone area, hardness and wear rate of AA6082 AMCs incorporating FSP parameters using statistical tools such as design of experiments, analysis of variance etc. SiC, Al$_2$O$_3$, TiC, B$_4$C and WC were used as reinforcements. The FSP experiments were conducted according to central composite design (CCD) [25–29].

2. Experimental procedure

2.1. Identification of process parameters

Fig. 1 lists the FSP parameters, which control the mechanical and tribological properties of AMCs. The major parameters that appreciably affect the properties are tool rotational speed (N), traverse speed (S), groove width (W) and type of ceramic particle (C) [18,20,22,30].

2.2. Finding the limits of the process parameters

The operational range of each identified process parameters were fixed based on several set of trial runs. Typical FSP defects such as tunnel, pin hole, worm hole etc were checked at the cross-section of trial specimens and crown appearance was examined for its smoothness. The limits of each factor were chosen so that the FSP zone is free from any kind of defects. The upper and lower limit of each factor was coded as +2 and –2 respectively to facilitate the recording and processing experimental data. The intermediate values were estimated using the following correlation.

$$X_i = 2[2X - (X_{max} + X_{min})]/(X_{max} - X_{min}) \qquad (1)$$

where X_i is the required coded value of a variable X; X is any value of the variable from X_{min} to X_{max}; X_{min} is the lowest level of the variable; X_{max} is the highest level of the variable. The selected levels and

process parameters with their units and notations are furnished in Table 1.

2.3. Developing the design matrix

A four factor, five level central composite rotatable factorial design consisting of 31 sets coded conditions with seven center points as given in Table 2 was applied to carry out the experiments. A comprehensive description of the design matrix is available elsewhere [31,32].

2.4. Production of AMCs as per design matrix

Aluminum alloy AA6082 plates of 100 mm length, 50 mm width and 10 mm thickness were used for this investigation. The electron backscatter diffraction (EBSD) map and composition of as received aluminum alloy is presented in Fig. 2 and Table 3 respectively. Grooves were machined at the center of the plate using wire EDM and packed with five kinds of ceramic particles such as Al$_2$O$_3$ (~10 μm), SiC (~8 μm), TiC (~2 μm), B$_4$C (~4 μm) and WC (~5 μm) as detailed in Table 1. The SEM micrographs of those ceramic particles are depicted in Fig. 3. A pinless tool was at first used to envelop the open end of grooves to avoid the particles from escaping during FSP. A tool having threaded profile and made of HCHCr steel as shown in Fig. 4 was used for this investigation. The tool had a shoulder diameter of 18 mm, pin diameter of 6 mm and pin length of 5.5 mm. The tool was oil hardened to 63 HRC. A single pass FSP was carried out semiautomatically on an indigenously built FSW machine (M/s RV Machine Tools, Coimbatore, India). A detailed description of FSP procedure is available in a published work [33]. FSP experiments were executed randomly as per the design matrix in Table 2 to remove any systematic errors creeping into the system. The friction stir processed plates are shown in Fig. 5.

Table 1
Friction stir processing parameters and their levels.

No	Parameter	Notation	Unit	Levels				
				–2	–1	0	1	2
1	Rotational speed	N	rpm	800	1000	1200	1400	1600
2	Traverse speed	S	mm/min	20	40	60	80	100
3	Groove width	W	mm	0	0.4	0.8	1.2	1.6
4	Ceramic powder	C	–	Al$_2$O$_3$	SiC	TiC	B$_4$C	WC

Table 2
Design matrix with its experimental results.

Trial run	FSW process parameters				FSP area (mm²)	Hardness (Hv)	Wear rate ($\times 10^{-5}$ mm³/m)
	N	S	W	C			
FSP01	−1	−1	−1	−1	58	96	482
FSP02	+1	−1	−1	−1	56	87	517
FSP03	−1	+1	−1	−1	51	104	410
FSP04	+1	+1	−1	−1	50	95	455
FSP05	−1	−1	+1	−1	43	117	379
FSP06	+1	−1	+1	−1	44	106	421
FSP07	−1	+1	+1	−1	38	131	319
FSP08	+1	+1	+1	−1	39	119	380
FSP09	−1	−1	−1	+1	52	99	474
FSP10	+1	−1	−1	+1	54	90	511
FSP11	−1	+1	−1	+1	52	107	428
FSP12	+1	+1	−1	+1	51	98	440
FSP13	−1	−1	+1	+1	41	120	372
FSP14	+1	−1	+1	+1	47	109	397
FSP15	−1	+1	+1	+1	37	135	316
FSP16	+1	+1	+1	+1	42	118	343
FSP17	−2	0	0	0	40	151	315
FSP18	+2	0	0	0	54	98	446
FSP19	0	−2	0	0	57	97	421
FSP20	0	+2	0	0	39	149	362
FSP21	0	0	−2	0	60	73	530
FSP22	0	0	+2	0	33	141	347
FSP23	0	0	0	−2	48	84	445
FSP24	0	0	0	+2	46	85	440
FSP25	0	0	0	0	48	121	417
FSP26	0	0	0	0	47	113	416
FSP27	0	0	0	0	47	115	421
FSP28	0	0	0	0	46	119	416
FSP29	0	0	0	0	48	114	414
FSP30	0	0	0	0	47	117	418
FSP31	0	0	0	0	48	112	424
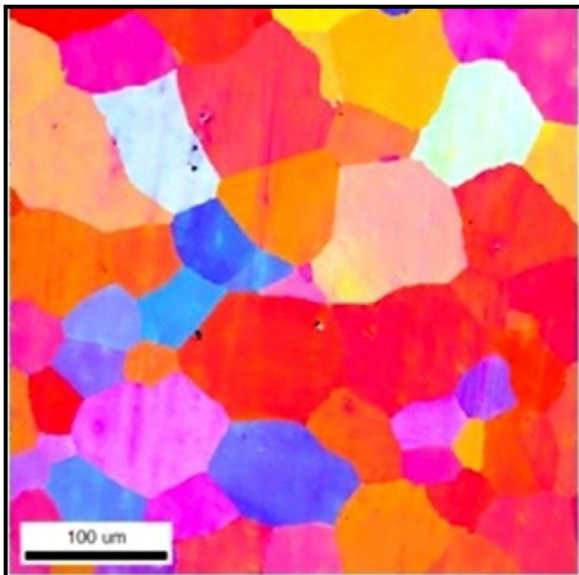
Fig. 2. EBSD (IPF + grain boundary) map of aluminum alloy AA6082.

2.5. Recording the response parameters

Specimens were machined from the friction stir processed plates to assess microstructure and microhardness. The specimens were thoroughly polished according to standard metallographic procedure and etched with Keller's reagent. The etched specimens were observed using a scanning electron microscope and EBSD. The digital image of the macrostructure of the etched specimens was captured using a digital optical scanner. The area of the FSP zone was computed using an image analyzer. The microhardness was recorded using a microhardness tester at 500 g load applied for 15 seconds at ten different locations within the FSP zone. The average value was taken to represent for each trial run. Care was taken not to land the indenter directly on the particles. Specimens of size 40 mm × 6 mm × 5 mm were prepared from the FSP zone using wire electric discharge machining (WEDM) to estimate wear rate. The wear rate of AMCs was measured using a pin-on-disc wear apparatus (DUCOM TR20-LE) at room temperature according to ASTM G99-04 standard. The wear test was conducted at a sliding velocity of 1 m/s, normal force of 25 N and sliding distance of 2500 m. The polished surface of the pin was slid on a hardened chromium steel disc. A computer aided data acquisition system was used to monitor the loss of height. The volumetric loss was computed by multiplying the cross-sectional area of the test pin with its loss of height. The wear rate was obtained by dividing volumetric loss to sliding distance.

Table 3
Chemical composition of AA6082 aluminum alloy.

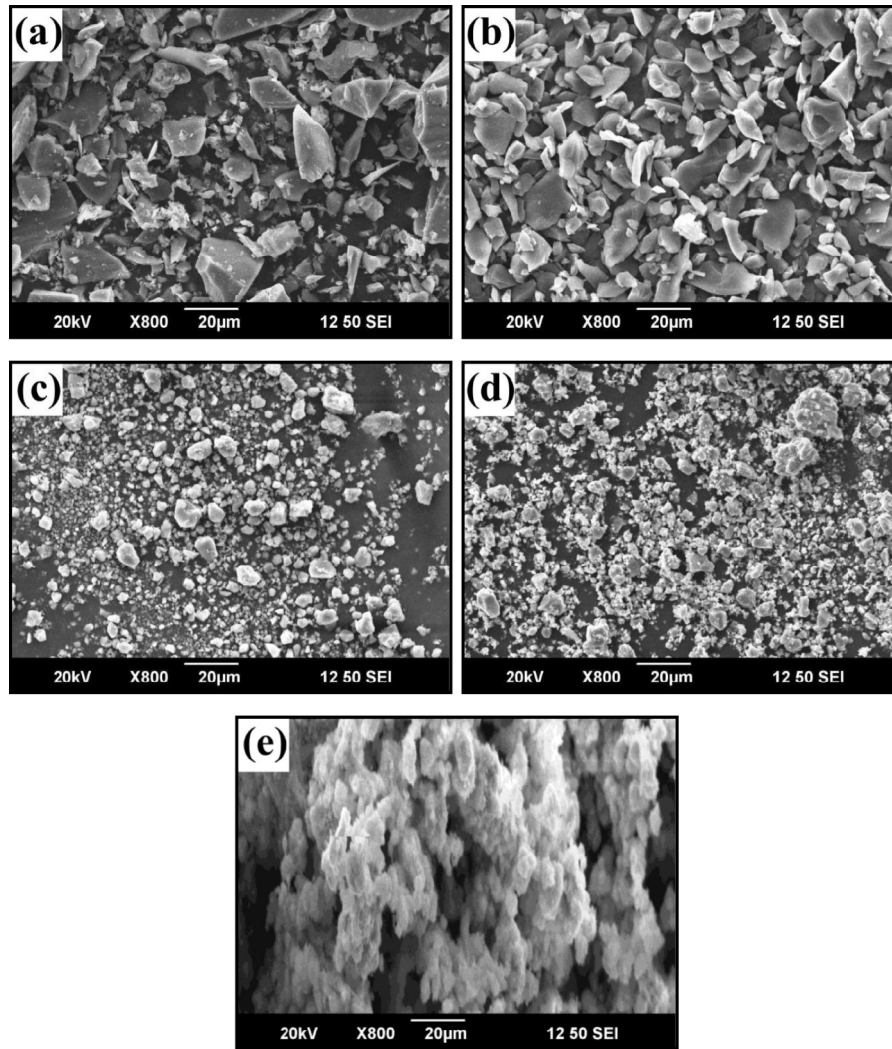| Element	Mg	Si	Fe	Mn	Cu	Cr	Zn	Ti	Aluminum
wt.%	0.78	1.06	0.21	0.55	0.09	0.03	0.06	0.01	Balance

Fig. 3. SEM micrograph of ceramic powders: (a) SiC, (b) Al_2O_3, (c) TiC, (d) B_4C and (e) WC.

2.6. Development of empirical relationships

The response functions representing the FSP area, microhardness and wear rate of AMCs are functions of rotational speed (N), traverse speed (S), groove width (W) and ceramic particles (C), which are stated as follows.

$$R = f(N, S, W, C) \tag{2}$$

The second order polynomial regression equation used to represent the response 'Y' for k factors is given by

$$Y = b_0 + \sum_{i=1}^{k} b_i x_i + \sum_{i=1}^{k} b_{ii} x_i^2 + \sum_{i=1}^{k} b_{ij} x_i x_j \tag{3}$$

The chosen polynomial for four factors is expressed for all the responses as follows.

$$R = b_0 + b_1 N + b_2 S + b_3 W + b_4 C + b_{11} N^2 + b_{22} S^2 + b_{33} W^2 + b_{44} C^2 + b_{12} NS + b_{13} NW + b_{14} NC + b_{23} SW + b_{24} SC + b_{34} WC \tag{4}$$

where b_0 is the average of responses and b_1, b_2, ... b_4, b_{11}, b_{22}, ... b_{44} are the response coefficients that depend on respective main and interaction effects of parameters. The coefficients were computed using the statistical software SYSTAT 12. The empirical relationships

were developed after estimating the coefficients. All the coefficients were tested for their significance level at 95% confidence level. The insignificant coefficients were removed without affecting the accuracy of the empirical relationships using Student t-test. The significant coefficients were taken into account to construct the final empirical relationships. The final developed empirical relationships with processing factors in coded form for all responses are given below.

$$\text{FSP Area} \, (mm^2) = 47.194 + 1.625N - 2.958S - 6.125W \tag{5}$$

$$\text{Microhardness} \, (HV) = 115.857 - 8.042N + 7.792S + 13.125W + 1.9N^2 + 1.525S^2 - 2.475W^2 - 8.1C^2 \tag{6}$$

$$\text{Wear rate} \, (\times 10^{-5} \, mm^3/m) = 418 + 22.75N - 24.167S - 48.167W - 9.042N^2 - 6.292S^2 + 5.458W^2 + 6.458C^2 \tag{7}$$

2.7. Checking the adequacy of the empirical relationships

The statistical outcomes of the developed empirical relationships are furnished in Table 4. The predicted empirical relationship

Fig. 4. Fabricated friction stir processing tool.

Table 4
Statistical results of the developed empirical relationships.

Response	R-square	Adjustable R-square	SE
FSP area	0.900	0.888	2.203
Microhardness	0.952	0.877	6.554
Wear rate	0.957	0.944	13.170

values will precisely match with the experimental results if the R-square value is 1. Higher values of 'R-square' and lower values of standard error (SE) show that the empirical relationships are adequate. The adequacy of the developed empirical relationships was analyzed for all the responses using analysis of variance (ANOVA) technique, which is given in Table 5. The value of calculated F ratios was higher than that of the tabulated values at 95% confidence level. Hence, the developed empirical relationships are quite adequate.

Further, the scatter diagrams as presented in Fig. 6 show that the actual and predicted values are scattered in both sides and close to 45° line, which prove the adequacy of the empirical relationships.

2.8. Validation of the empirical relationships

The conformity tests were performed to substantiate the validity of the developed empirical relationships. Five tests were carried out at different values of rotational speed, traverse speed, groove width and ceramic particles other than those used in the design matrix and their responses were calculated. The obtained results are presented in Table 6. The error in the prediction was calculated as per the expression given below. The percentage of error is within ±8%, which confirms the accuracy of the developed empirical relationships [25,31].

$$\text{Percentage error} = [(\text{experimental value} - \text{predicted value})/ \text{predicted value}] \times 100 \qquad (8)$$

3. Results and discussion

The influence of FSP process parameters (tool rotational speed, traverse speed, groove width and type of ceramic particle) on area of the stir zone, hardness and wear rate of AA6082 AMCs were deduced from the developed empirical relationships. The following sections attempt to explain the possible causes for the obtained trends and correlate with the observed microstructure.

3.1. Effect of tool rotational speed

Fig. 7 depicts the predicted trends of measured responses as a function of tool rotational speed for a constant set of traverse speed of 60 mm/min, groove width of 0.8 mm and ceramic particle of TiC. The area of the stir zone increases linearly (Fig. 7a) as tool rotational speed is increased from 800 rpm to 1600 rpm. The area of the stir zone was measured to be 44 mm^2 at rotational speed of 800 rpm and 51 mm^2 at rotational speed of 1600 rpm. The macrostructure of stir zone at different tool rotational speeds is given in Fig. 8a,b and i. The increase in the cross-sectional area of the stir zone with the increase in tool rotational speed is clearly seen. The tool rotational speed determines the amount of frictional heat produced during FSP [34]. Moghaddas and Bozorg [22] recorded the thermal profile during FSP to produce AA5754/Si$_3$N$_4$ AMCs. They observed an increase in peak temperature with an increase in tool rotational speed. The frictional heat is spent to plasticize the aluminum matrix. The higher the available frictional heat, the greater higher will be the plasticized aluminum. The frictional heat increases as tool rotation speed increases, consequently the amount of plasticized aluminum increases. Thus the area of the stir zone enlarges as tool rotational speed is increased from 800 rpm to 1600 rpm.

Fig. 9 reveals the SEM micrographs of AA6082 AMCs as a function of tool rotational speed. The distribution of the particles is influenced by the tool rotational speed. The distribution at 800 rpm

Table 5
ANOVA results of the developed empirical relationships.

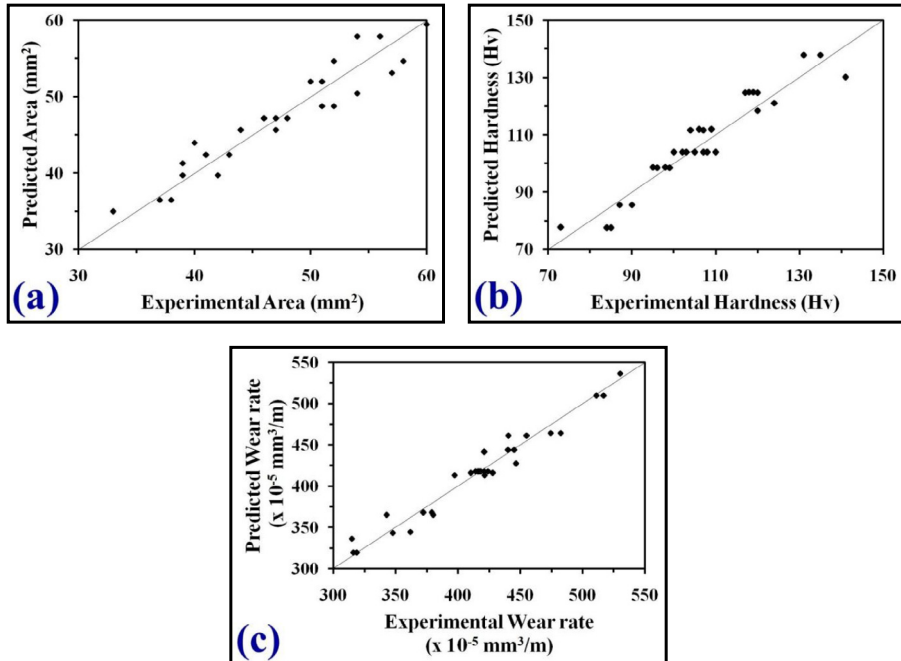| Response	Source	Sum of squares	Degrees of freedom	Mean-square	F-ratio (calculated)	F-ratio (tabulated)
FSP area	Regression	1173.792	3	391.264	80.613	2.96
	Residual	131.047	27	4.854		
Microhardness	Regression	10,732.996	7	1356.702	31.588	2.44
	Residual	994.875	23	42.950		
Wear rate	Regression	88,259.597	7	12,608.514	72.690	2.44
	Residual	3989.500	23	173.457		

Fig. 5. Friction stir processed plates.

Fig. 6. Scatter diagram for the developed empirical relationships.

Table 6
Results of conformity experiments.

Trial run	FSW process parameters				FSP area (mm^2)			Microhardness (HV)			Wear rate ($\times 10^{-5}$ mm^3/m)		
	N	S	W	C	Actual	Predicted	Error (%)	Actual	Predicted	Error (%)	Actual	Predicted	Error (%)
1	1.25	−1.5	−1.25	−2	58	61	−5.41	51	48	6.25	522	549	−4.91
2	0.75	−0.25	0.5	−1	49	46	6.31	100	107	−6.54	434	419	3.49
3	0.25	−0.75	1.5	0	43	41	5.83	117	123	4.87	398	378	5.36
4	−0.5	0.75	0.75	1	37	40	−6.49	119	127	−6.29	334	356	−6.21
5	−1.5	−1.25	−0.5	2	55	52	6.76	93	85	9.41	402	435	−7.63
Average							1.4			1.54			1.98

(Fig. 9a) is poor. Particles are closely packed in many regions. The distribution is fairly homogenous as tool rotational speed is increased to 1200 rpm. The distribution further improved at 1600 rpm. The increase in tool rotational speed increased the mean interparticle distance. Apart from frictional heat generation, tool rotation stirs the plasticized material around the pin and results in the transportation of the plasticized material across the stir zone. The material flow from advancing side to retreading side at 800 rpm is inadequate, causing poor distribution. The tool rotational speed is not sufficient to disperse the packed particles into all regions within the plasticized aluminum. The FSP process induces plastic strain on the processed aluminum. This plastic strain increases as tool rotation speed is increased. The enhanced plastic strain aids to disperse the particles further into the particles free regions. The agglomeration of particles fades away.

The microhardness of the AA6082 AMCs (Fig. 7b) decreases as tool rotational speed is increased from 800 to 1600 rpm. The microhardness was measured to be 158 HV at 800 rpm and 124 HV at 1600 rpm. The formation of particle clusters at 800 rpm induces higher variation in hardness across the stir zone. The indenter rested directly on the clusters as measurements were made at regular intervals. Therefore, the average hardness is higher at 800 rpm. The increase in tool rotational speed shatters the particle clusters and particles are distributed more homogenously in the aluminum matrix. Concurrently, the area of the stir zone increases with an increase in tool rotational speed. The increase in stir zone area leads

to drop in actual volume fraction of the particles. Because, the same quantity of particles compacted in the groove is to be distributed into larger amount of plasticized aluminum. Further the aluminum matrix is subjected to higher frictional heat with an increase in tool rotational speed, which causes softening [16,22]. This leads to drop in hardness of the AMCs as tool rotational speed is increased.

The wear rate of the AA6082 AMCs (Fig. 7c) increases as tool rotational speed is raised from 800 to 1600 rpm. The wear rate was estimated to be 315×10^{-5} mm^3/m at 800 rpm and 446×10^{-5} mm^3/m at 1600 rpm. According to Archard's law, the wear rate of metallic materials is inversely proportional to the hardness of the material [35]. The drop in microhardness of the AMCs weakens the ability to resist the removal of metal in course of sliding wear.

3.2. Effect of traverse speed

Fig. 10 shows the predicted trends on the properties of AA6082 AMCs as a function of traverse speed for a constant set of tool rotational speed of 1200 rpm, groove width of 0.8 mm and ceramic particle of TiC. The area of the stir zone (Fig. 10a) reduces linearly as the traverse speed is increased from 20 mm/min to 100 mm/min. The area of the stir zone was computed to be 45 mm^2 at lower traverse speed of 20 mm/min and 23 mm^2 at higher traverse speed of 60 mm/min. The macrostructure of stir zone at different traverse speed is depicted in Fig. 8c,d and i. It is evident that the area of the stir zone decreases with an increase in traverse speed. The rotational
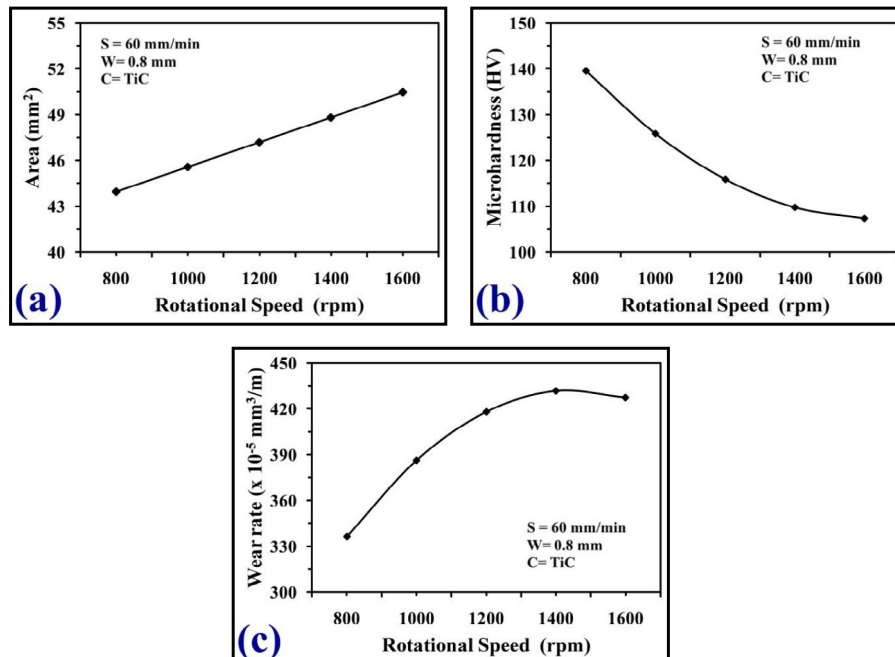

Fig. 7. Effect of tool rotational speed on (a) area of stir zone, (b) microhardness and (c) wear rate of AA6082 AMCs.
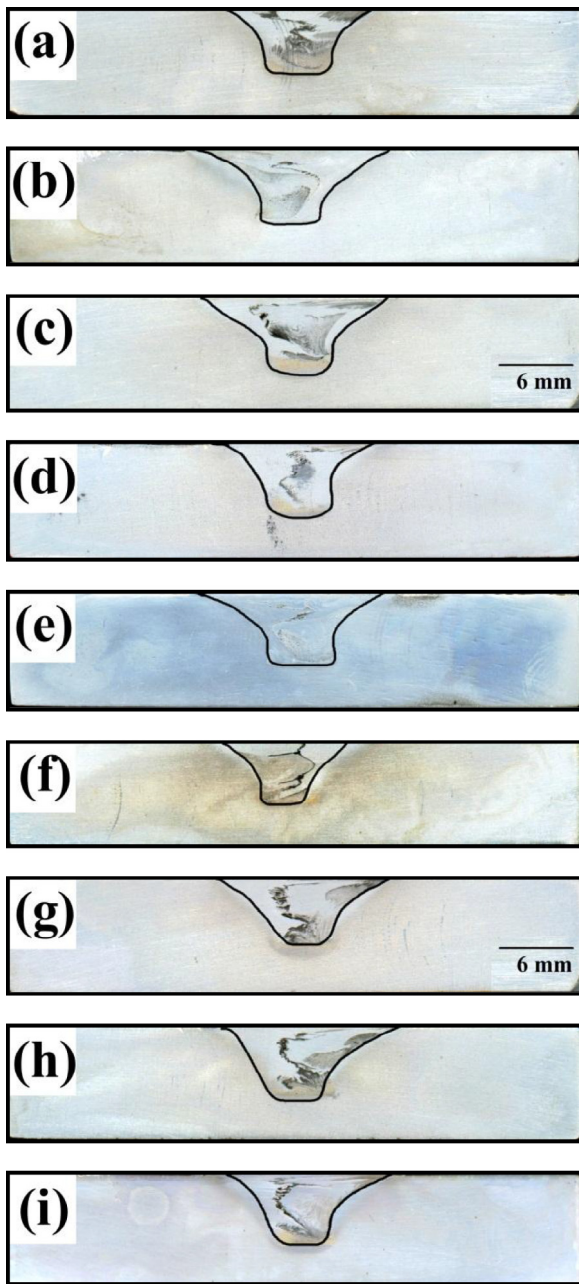
Fig. 8. Macrographs of AA6082 AMCs of trial runs: (a) FSP17 (N = 800 rpm, S = 60 mm/min, W = 0.8 mm, C = TiC), (b) FSP18 (N = 1600 rpm, S = 60 mm/min, W = 0.8 mm, C = TiC), (c) FSP19 (N = 1200 rpm, S = 20 mm/min, W = 0.8 mm, C = TiC), (d) FSP20 (N = 1200 rpm, S = 100 mm/min, W = 0.8 mm, C = TiC), (e) FSP21 (N = 1200 rpm, S = 60 mm/min, W = 0 mm, C = TiC), (f) FSP22 (N = 1200 rpm, S = 60 mm/min, W = 1.6 mm, C = TiC), (g) FSP23 (N = 1200 rpm, S = 60 mm/min, W = 0.8 mm, C = Al$_2$O$_3$), (h) FSP24 (N = 1200 rpm, S = 60 mm/min, W = 0.8 mm, C = WC) and (i) FSP25 (N = 1000 rpm, S = 60 mm/min, W = 0.8 mm, C = TiC).

motion of the tool generates frictional heat. The traverse speed controls the available frictional to unit length of FSP. It limits the residing time of frictional heat [36]. The residing time reduces as traverse speed increases and the quantity of available frictional heat is decreased. More aluminum is plasticized at traverse speed of 20 mm/min due higher residing time and availability of high frictional heat. The stir zone is broader. But the residing time is low at traverse speed of 100 mm/min and the amount of plasticized aluminum is low, resulting in smaller stir zone.

Fig. 11 reveals the SEM micrographs of AA6082 AMCs as a function of traverse speed. The micrographs indicate that the distribution is affected by the change in traverse speed. The distribution of particles is reasonably homogenous at 20 mm/min. No particle clusters is observed. But particles are closely packed and cluster of particles is also noticed at 100 mm/min. The increase in traverse speed reduced the average inter particle distance and caused the formation of particle clusters. The tendency to form particle clusters increased with an increase in traverse speed. The traverse speed not only dictates the residing time of frictional heat but also the available degree of tool rotation. The stirring action of the tool is vigorous at traverse speed of 20 mm/min, which induces high plastic strain on the aluminum matrix and disperses the particles effectively into the plasticized aluminum. The intense stirring and adequate material flow produces homogenous distribution. The available stirring action of the tool is inadequate at traverse speed of 100 mm/min and leads to improper mixing of particles and plasticized aluminum. Hence, the particles are closely located and clusters are formed.

The microhardness of the AA6082 AMCs (Fig. 10b) increases as traverse speed is raised from 20 mm/min to 100 mm/min. The microhardness was estimated to be 120 HV at 20 mm/min and 157 HV at 100 mm/min. The actual volume fraction of particles is low at traverse speed of 20 mm/min due to higher amount of plasticized material and larger stir zone area. The decrease in interparticle distance with an increase in traverse speed raises the hardness of the AMCs. The wear rate of the AA6082 AMCs (Fig. 10c) decreases as traverse speed is raised from 20 mm/min to 100 mm/min. The wear rate was computed to be 421×10^{-5} mm^3/m at 20 mm/min and 362×10^{-5} mm^3/m at 100 mm/min. The composite provides resistance to removal of metal during sliding wear due to an increase in hardness. Therefore, the wear rate reduces with an increase in tool traverse speed.

3.3. Effect of groove width

Fig. 12 shows the predicted trends of measured responses as a function of groove width for a constant set of tool rotational speed of 1200 rpm, traverse speed of 60 mm/min and ceramic particle of TiC. The area of the stir zone decreases linearly as groove width is increased from 0 mm to 1.6 mm. The area of the stir zone was assessed to be 60 mm^2 at zero groove width and 33 mm^2 at groove width of 1.6 mm. The macrostructure of stir zone at different groove width is depicted in Fig. 8e,f and i. It is visible from the macrostructures that the area of the stir zone diminishes as groove width is increased. The possible causes for the reduction in stir zone area can be attributed to the following factors. First, the quantity of compacted particles increases with increase in groove width. Second, the quantity of aluminum available for plasticization reduces. The flow stress of the plasticized composite increases as the quantity of particles is increased. The ceramic particles are non-deformable, which inhibit the free flow of plasticized aluminum. Moreover, the decrease in available aluminum enhances the volume fraction of particles in the AMCs. Subsequently, the flow stress of the composite increases further. Therefore, the area of the stir zone reduces as groove width is increased.

Fig. 13 reveals the EBSD and SEM micrographs of AA6082 AMCs as a function of groove width. Zero groove width corresponds to friction stir processed aluminum alloy AA6082. The EBSD map (Fig. 13a) shows the presence of fine grains compared to coarse grain size of AA6082 prior to FSP (Fig. 2). The generation of fine grains can be attributed to dynamic recrystallization [37]. The distribution of ceramic particles (Fig. 13b and c) in the aluminum matrix is homogenous irrespective of groove width. As groove width is increased, the number of particles increases in addition to reduction in average interparticle spacing. The homogenous distribution is a
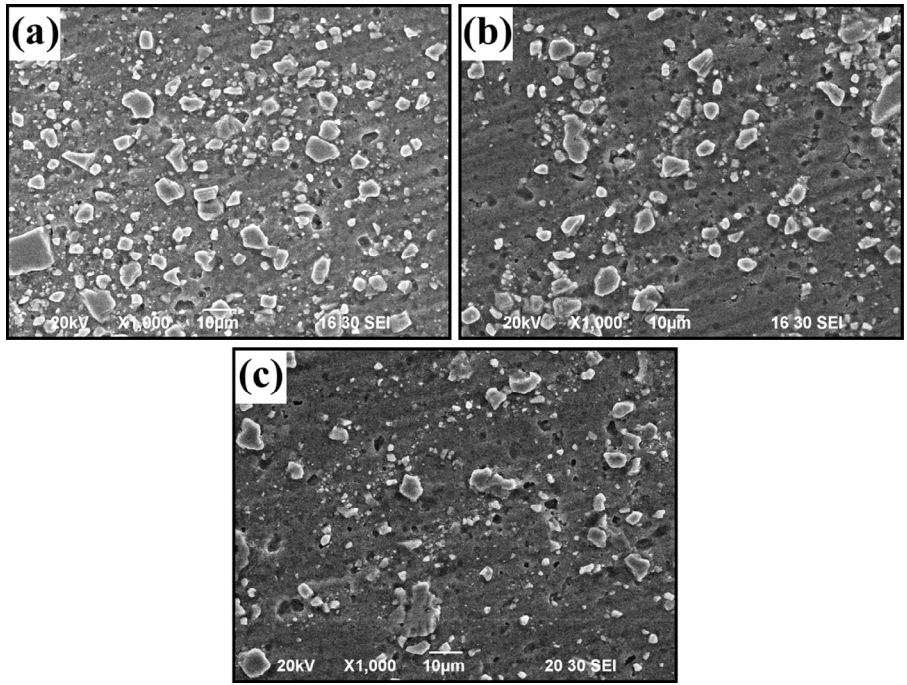
Fig. 9. SEM micrographs of AA6082 AMCs at tool rotational speed of (a) 800 rpm (FSP17), (b) 1000 rpm (FSP25) and (c) 1600 rpm (FSP18).

result of sufficient generation of frictional heat, stirring of plasticized composite and material flow across the stir zone. The number of particle clusters is limited to few. The raise in volume fraction of particles with an increase in groove width reduces the average interparticle spacing.

The microhardness of the AA6082 AMCs (Fig. 12b) increases as groove width is increased from 0 mm to 1.6 mm. The microhardness was found to be 73 HV at 0 mm and 141 HV at 1.6 mm. The presence of second phase ceramic particles contributes to an increase in dislocation density of aluminum. The microhardness is increased

as a result of interaction between particles and dislocations. The dislocation density increases as groove width is increased due to increase in number of particles. Therefore, the interaction between particles and dislocations further go up enhancing the hardness of the composite. The wear rate of the AA6082 AMCs (Fig. 12c) decreases as groove width is increased from 0 mm to 1.6 mm. The wear rate was estimated to be 530×10^{-5} mm³/m at 0 mm and 347×10^{-5} mm³/m at 1.6 mm. The enhancement of hardness of the composites retards the removal of material during sliding wear. Thus, the wear rate is reduced as groove width is increased.
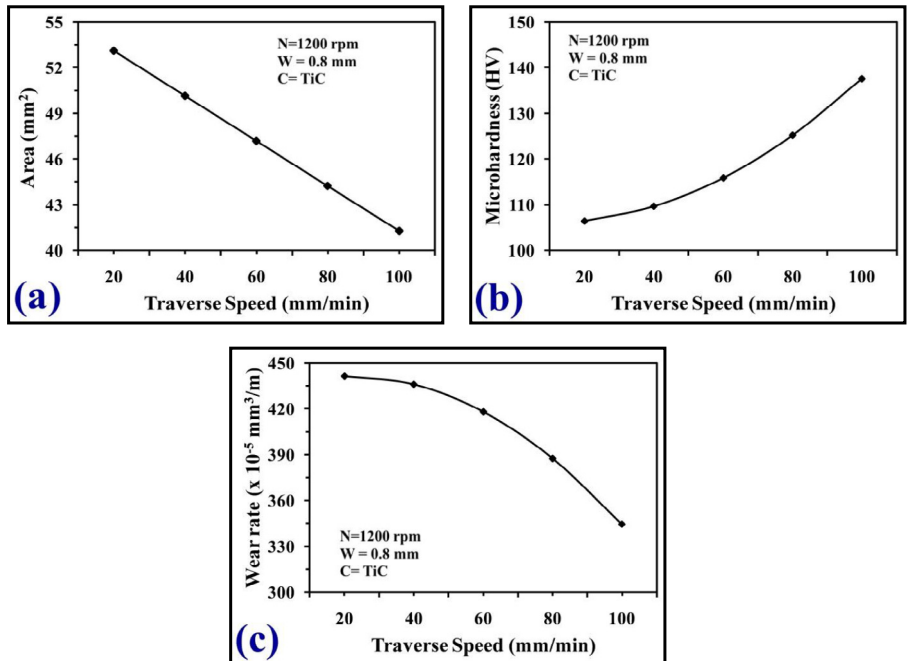

Fig. 10. Effect of traverse speed on (a) area of stir zone, (b) microhardness and (c) wear rate of AA6082 AMCs.
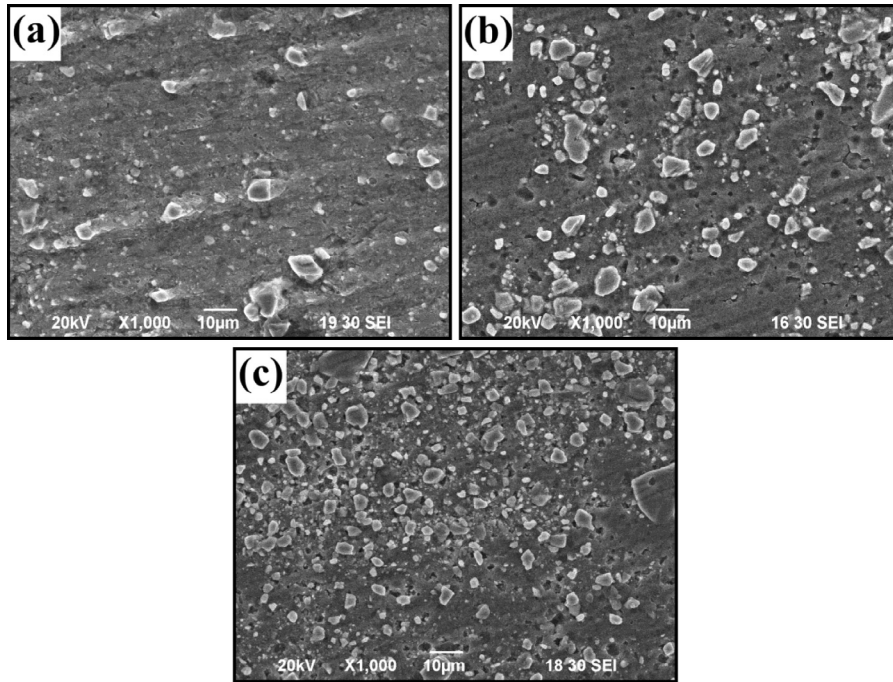
Fig. 11. SEM micrographs of AA6082 AMCs at traverse speed of (a) 20 mm/min (FSP19), (b) 60 mm/min (FSP25) and (c) 100 mm/min (FSP20).

3.4. Effect of ceramic particles

Fig. 14 shows the predicted trends on the properties of AA6082 AMCs as a function of type of ceramic particles for a constant set of tool rotational speed of 1200 rpm, traverse speed of 60 mm/min and groove width of 0.8 mm. The developed empirical relationship in Equation (5) to predict the area of the stir zone does not have the ceramic particle term. It means that the value of ceramic particle coefficient is insignificant and does not affect the area of the stir zone. The macrostructure of stir zone at different ceramic particle type is presented in Fig. 8g,h and i. The variation in the area of stir zone is negligible for a set of FSP parameters. This result is attributed to insignificant variation in the flow stress of plasticized aluminum with various kinds of ceramic particles. Figs. 13b and 15 reveal the SEM micrographs of AA6082 AMCs as a function of type of ceramic particle. It is remarkable to notice a homogeneous distribution of particles regardless of the type of ceramic particle. The distribution is not a function of type of ceramic particle. It can be concluded that the FSP process is insensitive to the type of ceramic particle. It is nearly impossible to produce AMCs
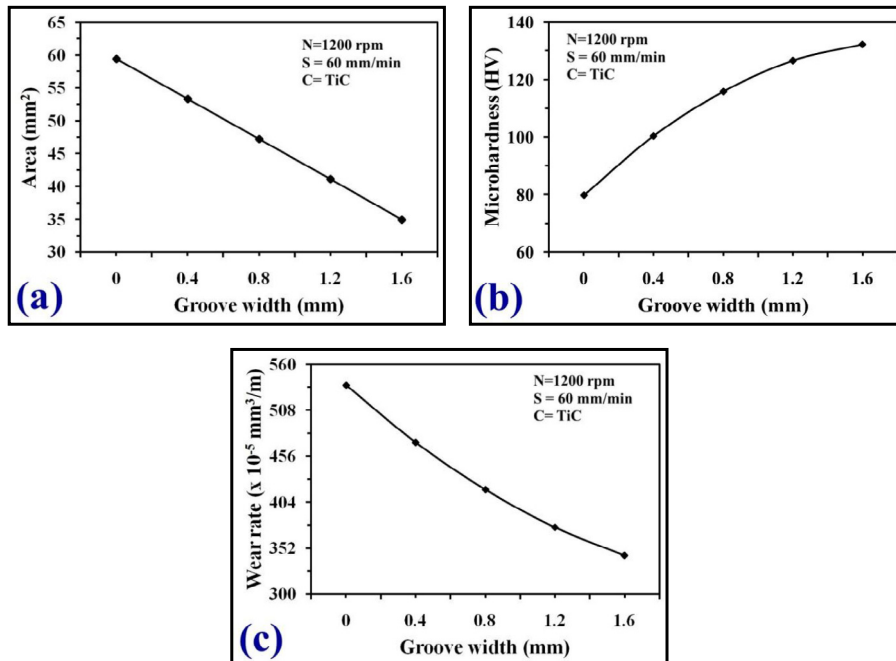

Fig. 12. Effect of groove width on (a) area of stir zone, (b) microhardness and (c) wear rate of AA6082 AMCs.
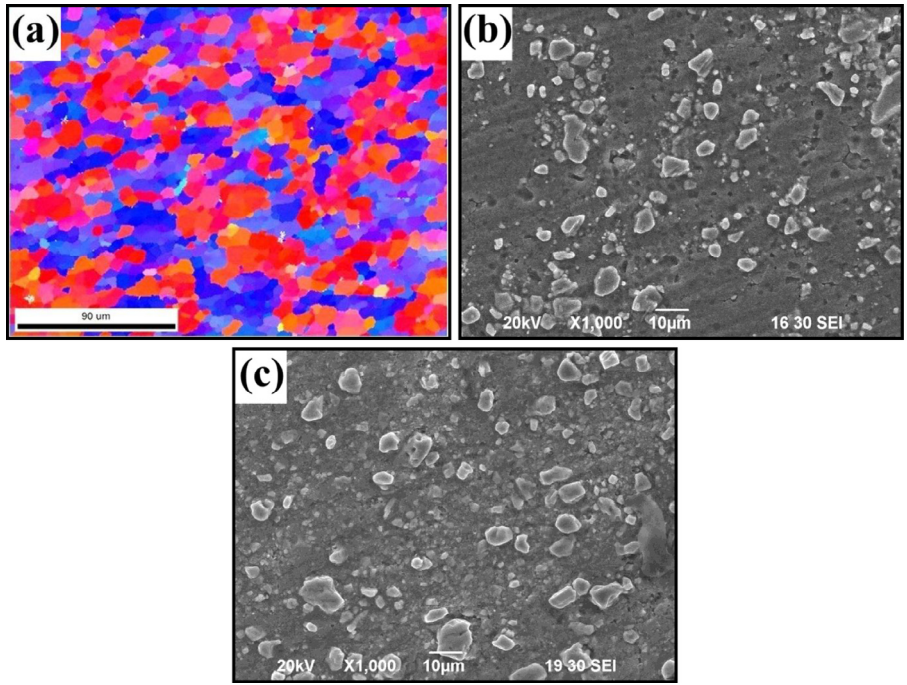
Fig. 13. SEM micrographs of AA6082 AMCs at groove width of (a) 0 mm (EBSD map, FSP21), (b) 0.8 mm (FSP25) and (c) 1.6 mm (FSP22).

reinforced with different kinds of ceramic particles by applying conventional liquid metallurgy routes. The distribution depends on the wettability between the ceramic particle and the molten aluminum as well as density gradient [9]. It is evident from EBSD grain distribution maps (Fig. 16) that the grain size variation is also negligible among various ceramic particles. The hardness of SiC, Al_2O_3,

TiC, B_4C and WC are respectively 2480 HK, 2100 HK, 2470 HK, 2750 HK and 1880 HK. Nevertheless, AA60682 AMCs reinforced with TiC particles exhibited higher microhardness and lowest wear rate, which can be reasoned as follows. There are several factors that control the properties of AMCs including size, shape, volume fraction, nature of distribution and type of ceramic particles [38]. TiC
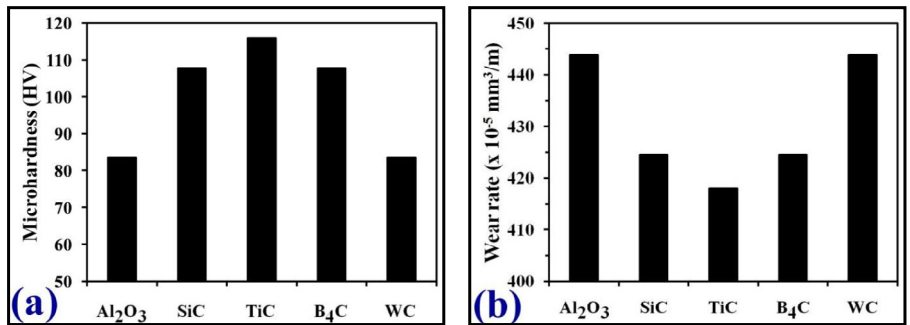

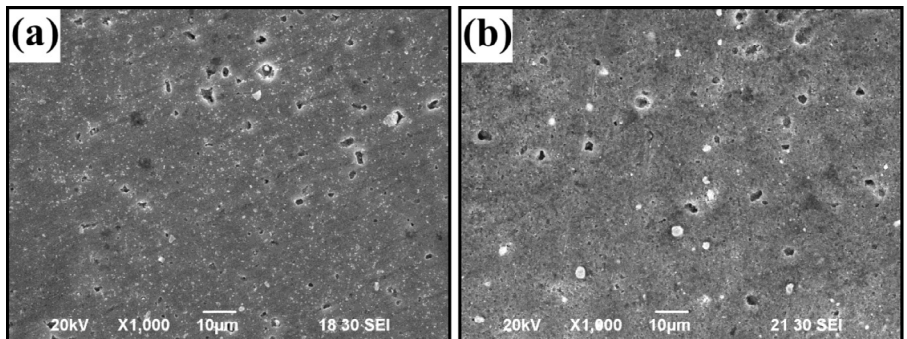**Fig. 14.** Effect of ceramic powders on (a) microhardness and (b) wear rate of AA6082 AMCs.

Fig. 15. SEM micrographs of AA6082 AMCs reinforced with (a) Al_2O_3 (FSP23) and (b) WC (FSP24).
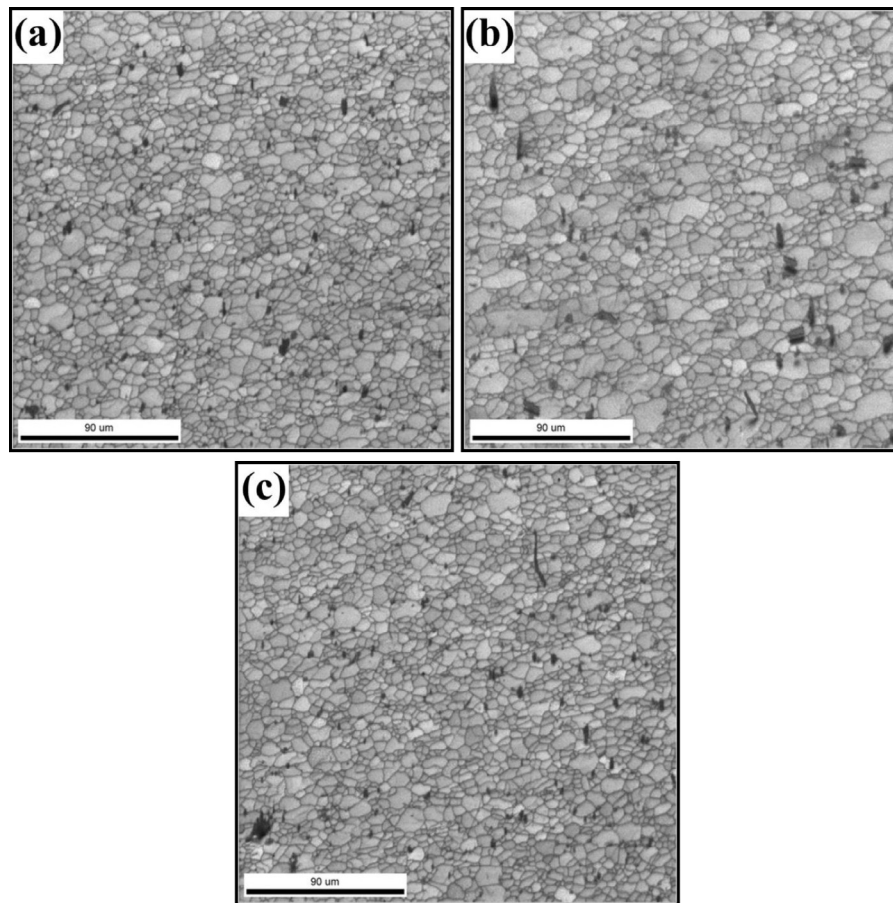
Fig. 16. EBSD grain boundary maps of AA6082 AMCs reinforced with (a) Al_2O_3 (FSP23), (b) TiC (FSP25) and (c) WC (FSP24).

particles were characterized with a spherical morphology and showed lower particle size in comparison to other ceramic particles considered for this research work. The hardness of B_4C particles are higher compared to TiC particles. But, the hardness of AA6082/B_4C AMC is lower to that of AA6082/TiC AMC. This can be attributed to fine size, which lowers the interparticle distance and improves the hardness of the matrix. Therefore, AA6082 AMCs reinforced with TiC particles manifest higher microhardness and lower wear rate.

4. Conclusions

AA6082 AMCs reinforced with various ceramic particles were effectively produced using the novel solid state method FSP. Empirical relationships were estimated to predict the influence of FSP parameters on the properties of AA6082. The area of the stir zone that contained the composite was influenced by tool rotational speed, traverse speed and groove width. The microhardness and wear rate were significantly affected by the four FSP parameters considered in this work. The area of the stir zone was maximum at higher tool rotational speed, lower traverse speed and minimum groove width. The distribution of second phase ceramic particles was finer at higher tool rotational speed and lower traverse speed. The distribution was unaltered by the variation in groove width and type of ceramic particle. Higher microhardness and lower wear rate were observed at lower tool rotational speed, higher traverse speed, maximum groove width and TiC ceramic particle.

References

[1] K.K. Alaneme, K.O. Sanusi, Microstructural characteristics, mechanical and wear behaviour of aluminium matrix hybrid composites reinforced with alumina, rice husk ash and graphite, Eng. Sci. Technol. Int. J. 18 (2015) 416–422.
[2] R.D. Lara, N. Soltani, A. Bahrami, E.G. Castañeda, E.G. Sánchez, M.A.L.H. Rodríguez, Tribological characterization of Al7075–graphite composites fabricated by mechanical alloying and hot extrusion, Mater. Des. 67 (2015) 224–231.
[3] H. Liu, Y. Hu, Y. Zhao, H. Fujii, Microstructure and mechanical properties of friction stir welded AC4A + 30 vol.%SiCp composite, Mater. Des. 65 (2015) 395–400.
[4] C. Shoba, N. Ramanaiah, D. Nageswara Rao, Effect of reinforcement on the cutting forces while machining metal matrix composites – An experimental approach, Eng. Sci. Technol. Int. J. 18 (2015) 658–663.
[5] M.K. Akbari, O. Mirzaee, H.R. Baharvandi, Fabrication and study on mechanical properties and fracture behavior of nanometric Al_2O_3 particle-reinforced A356 composites focusing on the parameters of vortex method, Mater. Des. 46 (2013) 199–205.
[6] M.K. Akbari, H.R. Baharvandi, K. Shirvanimoghaddam, Tensile and fracture behavior of nano/micro TiB_2 particle reinforced casting A356 aluminum alloy composites, Mater. Des. 66 (2015) 150–161.
[7] B.S. Yigezu, P.K. Jha, M.M. Mahapatra, The key attributes of synthesizing ceramic particulate reinforced Al-based matrix composites through stir casting process: a review, Mater. Manuf. Process. 28 (2013) 969–979.

[8] M.A. Taha, Practicalization of cast metal matrix composites (MMCCs), Mater. Des. 22 (2001) 431–441.

[9] J. Hashim, L. Looney, M.S.J. Hashmi, Metal matrix composites: production by the stir casting method, J. Mater. Process. Technol. 92–93 (1999) 1–7.

[10] Z.Y. Ma, Friction stir processing technology: a review, Metallogr. Mater. Trans. A 39 (2008) 642–658.

[11] H.S. Arora, H. Singh, B.K. Dhindaw, Composite fabrication using friction stir processing – a review, Int. J. Adv. Manuf. Technol. 61 (2012) 1043–1055.

[12] R.S. Mishra, Z.Y. Ma, I. Charit, Friction stir processing: a novel technique for fabrication of surface composite, Mater. Sci. Eng. A 341 (2003) 307–310.

[13] Q. Liu, L. Ke, F. Liu, C. Huang, L. Xing, Microstructure and mechanical property of multi-walled carbon nanotubes reinforced aluminum matrix composites fabricated by friction stir processing, Mater. Des. 45 (2013) 343–348.

[14] M.S. Khorrami, M. Kazeminezhad, A.H. Kokabi, Thermal stability of aluminum after friction stir processing with SiC nanoparticles, Mater. Des. 80 (2015) 41–50.

[15] M.N.A. Fènoël, A. Simar, R. Shabadi, R. Taillard, B. De Meester, Characterization of oxide dispersion strengthened copper based materials developed by friction stir processing, Mater. Des. 60 (2014) 343–357.

[16] V. Sharma, U. Prakash, B.V.M. Kumar, Surface composites by friction stir processing: a review, J. Mater. Process. Technol. 224 (2015) 117–134.

[17] M. Salehi, H. Farnoush, J.A. Mohandesi, Fabrication and characterization of functionally graded Al–SiC nanocomposite by using a novel multistep friction stir processing, Mater. Des. 63 (2014) 419–426.

[18] E.R.I. Mahmoud, K. Ikeuchi, M. Takahashi, Fabrication of SiC particle reinforced composite on aluminium surface by friction stir processing, Sci. Technol. Weld. Joining 13 (2008) 607–618.

[19] D.K. Lim, T. Shibayanagi, A.P. Gerlich, Synthesis of multi-walled CNT reinforced aluminium alloy composite via friction stir processing, Mater. Sci. Eng. 507 (2009) 194–199.

[20] A. Kurt, I. Uygur, E. Cete, Surface modification of aluminium by friction stir processing, J. Mater. Process. Technol. 211 (2011) 313–317.

[21] M. Salehi, M. Saadatmand, J.A. Mohandesi, Optimization of process parameters for producing AA6061/SiC nanocomposites by friction stir processing, Trans. Nonferrous Met. Soc. China 22 (2012) 1055–1063.

[22] M.A. Moghaddas, S.F.K. Bozorg, Effects of thermal conditions on microstructure in nanocomposite of Al/Si₃N₄ produced by friction stir processing, Mater. Sci. Eng. A 559 (2013) 187–193.

[23] A. Devaraju, A. Kumar, B. Kotiveerachari, Influence of rotational speed and reinforcements on wear and mechanical properties of aluminum hybrid composites via friction stir processing, Mater. Des. 45 (2013) 576–585.

[24] M. Bahrami, K. Dehghani, M.K.B. Givi, A novel approach to develop aluminum matrix nano-composite employing friction stir welding technique, Mater. Des. 53 (2014) 217–225.

[25] N. Murugan, B. Ashok Kumar, Prediction of tensile strength of friction stir welded stir cast AA6061-T6/AlNp composite, Mater. Des. 51 (2013) 998–1007.

[26] V. Vasugi, K. Ramamurthy, Identification of design parameters influencing manufacture and properties of cold-bonded pond ash aggregate, Mater. Des. 54 (2014) 264–278.

[27] L. Qian, Y. Ping, L. Yunbai, Response surface modeling and optimization of a new impact-toughened mould material used in the shaping of sanitary ware, Mater. Des. 50 (2013) 191–197.

[28] N. Sadeghian, M.K.B. Givi, Experimental optimization of the mechanical properties of friction stir welded Acrylonitrile Butadiene Styrene sheets, Mater. Des. 67 (2015) 145–153.

[29] A.R. Rose, K. Manisekar, V. Balasubramanian, S. Rajakumar, Prediction and optimization of pulsed current tungsten inert gas welding parameters to attain maximum tensile strength in AZ61A magnesium alloy, Mater. Des. 37 (2012) 334–348.

[30] M. Azizieh, A.H. Kokabi, P. Abachi, Effect of rotational speed and probe profile on microstructure and hardness of AZ31/Al₂O₃ nanocomposites fabricated by friction stir processing, Mater. Des. 32 (2011) 2034–2041.

[31] D.G. Montgomery, Design and Analysis of Experiments, Wiley, Hoboken, 2001.

[32] G.E.P. Box, W.H. Hunter, J.S. Hunter, Statistics for Experiments, Wiley, New York, 1978.

[33] C.J. Lee, J.C. Huang, P.J. Hsieh, Mg based nano-composites fabricated by friction stir processing, Scr. Mater. 54 (2006) 1415–1420.

[34] S. Rajakumar, C. Muralidharan, V. Balasubramanian, Influence of friction stir welding process and tool parameters on strength properties of AA7075-T6 aluminium alloy joints, Mater. Des. 32 (2011) 535–549.

[35] A. Mandal, M. Chakraborty, B.S. Murty, Effect of TiB2 particles on sliding wear behaviour of Al–4Cu alloy, Wear 262 (2007) 160–166.

[36] S. Rajakumar, V. Balasubramanian, Correlation between weld nugget grain size, weld nugget hardness and tensile strength of friction stir welded commercial grade aluminium alloy joints, Mater. Des. 34 (2012) 242–251.

[37] R.S. Mishra, Z.Y. Ma, Friction stir welding and processing, Mater. Sci. Eng. R 50 (2005) 1–78.

[38] A.P. Sannino, H.J. Rack, Dry sliding wear of discontinuously reinforced aluminum composites: review and discussion, Wear 189 (1995) 1–19.